Pathology - Research and Practice 255 (2024) 155163

Contents lists available at ScienceDirect

Pathology - Research and Practice

journal homepage: www.elsevier.com/locate/prp

Histopathologic and immunophenotypic characterization of patient-derived pediatric malignant hepatocellular tumor xenografts (PDXs)

Kalyani R. Patel [a,*], Andres F. Espinoza [b], Martin Urbicain [c], Roma H. Patel [b], Angela Major [a], Stephen F. Sarabia [c], Dolores Lopez-Terrada [c], Sanjeev A. Vasudevan [b], Sarah E. Woodfield [b]

[a] Department of Pathology and Immunology, Anatomic Pathology Division, Texas Children's Hospital and Baylor College of Medicine, Houston, TX, USA
[b] Department of General Surgery, Division of Pediatric Surgery, Texas Children's Hospital and Baylor College of Medicine, Houston, TX, USA
[c] Department of Pathology and Immunology, Genomic Medicine Division, Texas Children's Hospital and Baylor College of Medicine, Houston, TX, USA

ARTICLE INFO

Keywords:
Xenograft
Pediatric
Liver
Hepatoblastoma
Histopathology
Immunohistochemistry

ABSTRACT

Advances in targeted therapies for pediatric hepatocellular tumors have been limited due to a paucity of clinically relevant models. Establishment and validation of intrahepatic patient-derived xenograft (PDX) models would help bridging this gap. The aim of this study is to compare the histomorphologic and immunophenotypic fidelity of patient tumors and their corresponding intrahepatic PDX models. Murine PDX models were established by intrahepatic implantation of patient tumors. Pathology slides from both patients and their corresponding PDX models were reviewed and quantitatively assessed for various histologic components and immunophenotypic markers. Ten PDX models were successfully established from nine patients with pre- (n=3) and post- (n=6) chemotherapy samples; diagnosed of hepatoblastoma (n=8) and hepatocellular neoplasm, not otherwise specified (n=1). Two of nine (22.2%) patients showed ≥75% fetal component; however, the corresponding PDX models did not maintain this fetal differentiation. High grade histology was seen in three patients (33.3%) and overrepresented in six PDX models (60%). Within the subset of three PDXs that were further characterized, significant IHC concordance was seen in all 3 models for CK7, CK19, Ki-67, and p53; and 2 of 3 models for Sox9 and Beta-catenin. GPC-3 and GS showed variable to moderate concordance, while Hepar was the least concordant. Our study shows that in general, the PDX models appear to represent the higher-grade component of the original tumor and show significant concordance for Ki-67, making them appropriate tools for testing new therapies for the most aggressive, therapy-resistant tumors.

1. Introduction

Hepatoblastoma (HB) is the most common primary liver malignancy in children, with an estimated incidence of 1.7 cases per million [1]. Hepatocellular neoplasm, not otherwise specified (HCN, NOS) is a provisional category to include malignant liver tumors, with histologic features of both HB and hepatocellular carcinoma (HCC), more frequently seen in children older than 5 years of age [2]. Standard management includes primary resection or chemotherapy followed by resection with a 3-year survival rate of 91% for standard-risk tumors [3]. High-risk cases are determined by pretreatment extent of disease (PRETEXT), age of diagnosis, levels of alpha-feto protein (AFP), vascular invasion, tumor rupture, extrahepatic extension of disease, multifocality of tumor, and metastases [24]. Patients that have high-risk disease have a lower 3-year survival of 65% [4]. High-risk cases require aggressive chemotherapy, leading to significant short and long-term complications, including deafness, cardiotoxicity, and renal toxicity [5–7]. Advances in targeted therapy are limited to the availability of representative samples for laboratory studies and tumor models. Few cell lines, such as HepG2, Huh-6, and HepT1, are available for experimental studies [8–10]. Earliest animal models were generated by subcutaneous injection of fresh patient-derived tumor cells in the back of female nude (Balb/c nun/nu) mice [8]. These subcutaneous murine models had several advantages, such as ease of access to monitor tumor growth and sampling

* Correspondence to: Department of Pathology and Immunology, Texas Children's Hospital and Baylor College of Medicine, 6621 Fannin St, Houston, TX 77030, USA .
E-mail address: krpatel@texaschildrens.org (K.R. Patel).

https://doi.org/10.1016/j.prp.2024.155163
Received 30 December 2023; Accepted 20 January 2024
Available online 1 February 2024

for various experimental studies. However, they did not recapitulate the tumor microenvironment or show distant metastasis. This was followed by models generated with splenic [9] and intrahepatic [10,11] injections of widely available cell lines. Both methodologies were successful in the development of intrahepatic tumors with the appropriate microenvironment. Splenic models typically resulted in small, multifocal nodules without a dominant mass, making it challenging to quantify the tumor burden and to study the effects of chemotherapy. Intrahepatic injection models did result in a dominant mass and, among other things, showed the ability to study drug toxicities in the context of impaired hepatic clearance due to tumor-related biliary obstruction – which was not possible in other models listed above. Recent developments in patient-derived xenograft (PDX) models are attempting to bridge this gap, leading to the identification of several novel candidate drugs for therapy-resistant tumors [12]. Limited studies have shown PDX models to be representative of original patient tumor samples with respect to histology and genetics [13]. However, the same report mentions that 12 out of 51 models (23.5%) showed discordance between the patient and the PDX histology with the PDX model mostly or exclusively representing the undifferentiated component in cases of rhabdomyosarcoma and nephroblastoma. Our study compared the histomorphologic and immunophenotypic profile of paired patient and corresponding PDX models of pediatric malignant liver tumors in order to evaluate and validate the models for future preclinical studies.

2. Methods

Samples were collected from patients after informed consent was obtained from their parents or guardians via an Institutional Review Board (IRB)-approved tissue collection protocol H-38834. All experiments on patient samples were performed in compliance with the Helsinki Declaration and approved by the Baylor College of Medicine IRB. All animal procedures used in this study were performed under an animal protocol approved by the Institutional Care and Use Committee of Baylor College of Medicine (AN-6191). A portion of viable tumor was harvested by a pathologist based on gross examination and placed in RPMI medium (cat. no. CM059–050, GenDEPOT, Katy, TX, USA) within approximately 30 min of surgical removal. Tumors were then implanted within 24 h as 6–8 mm^3 whole pieces into the livers of 6- to 12-week-old NSG immunocompromised animals (NOD.Cg-Prkdcscid Il2rgtm1Wjl/SzJ, Jackson Laboratory, Bar Harbor, ME, USA) as previously described [11]. Mice implanted with the tumor sample harvested directly from the patient were termed P0. When tumors began to impact animal health or when estimated tumor size by MRI reached criteria for euthanasia as described in our IACUC-approved animal protocol, animals were euthanized, and tumor was serially passaged into subsequent NSG immunocompromised animals for continued growth, as P1, P2, P3 etc. (Fig. 1).

All H&E slides were reviewed on the patient and corresponding PDX samples with quantitative assessment of various tumor components such as fetal, embryonal, mesenchymal, teratoid, and pleomorphic. Mitoses were identified per 10 high powered fields (hpf). The pleomorphic component was identified based on one or more of the following features: large tumor cells with nucleomegaly, hyperchromasia, irregular nuclear contours, prominent nucleoli, intranuclear inclusions, and atypical mitotic figures. Significant pleomorphism was defined as pleomorphic cells occupying > 50% of sampled tumor area. Select PDXs were chosen for further immunohistochemistry (IHC) analysis with

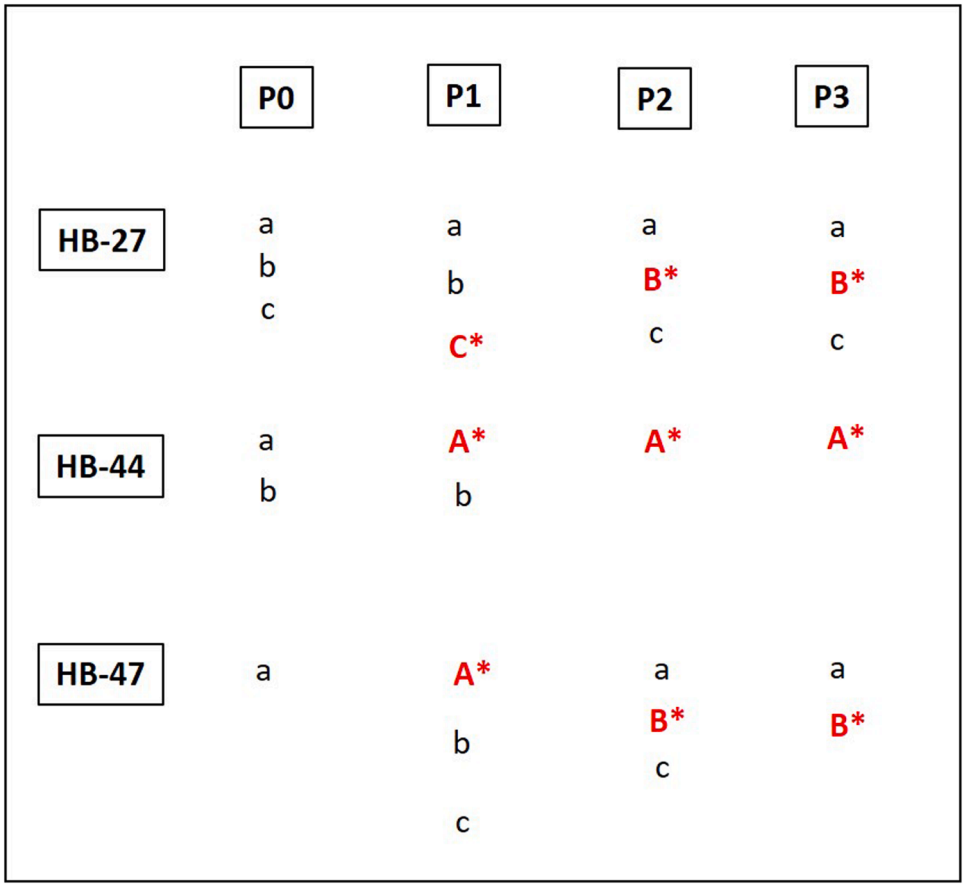

Fig. 1. PDX passaging workflow (HB-27, HB-44, and HB-47). Mice implanted directly with patient tumor are termed P0 with each letter (a,b,c) representing a different animal. Red font indicates the mouse whose tumor was passaged to later generations. P1 is the first passaged generation, followed by P2 and P3. * shows implanted tumors that were evaluated for immunohistochemistry.

three consecutive passages from each PDX namely P1, P2, and P3. (Fig. 1). IHC was used for Beta catenin (Leica, 17C2, RTU), Glypican-3 (GPC3) (Leica, 1G12 Mab, RTU), AFP (Invitrogen, ZSA06, 1:600), Glutamine synthetase (GS) (Abcam, 1:2500), Arginase (Abcam, SP156, 1:100), CK7 (Dako, OV-TL 12/30, 1:100), CK19 (Dako, RCK108, 1:2000), Hepar (Dako, OCH1E5, 1:50), Sox9 (Milipore, 1:1000), Ki67 (Dako, MIB-1, 1:50), EPCAM (Abcam, E144, 1:200), and p53 (Dako, DO-7, 1:50). IHC was scored as negative (score 0), < 1% cells positive (score 1), 1 to 25% positive (score 2), 25 to 75% positive (score 3), > 75% positive (score 4). Significant concordance was defined as all 3 generations of PDX showing a score of + /- 1 of the corresponding patient sample and moderate concordance as 2 of 3 generations with a score of + /- 1 of the corresponding patient sample.

3. Results

Tumor samples from nine patients were implanted to generate ten PDX models with a male to female ratio of 8:1. Age at tissue sampling for PDX development ranged from 1.3 to 7 years (mean 3.5 years). PDX models were created from two pre-therapy biopsies, one pre-therapy resection, four post-therapy resections, and two relapse samples. PDX models derived from the four post-therapy resections possibly represented tumor cells that were resistant to therapy. Primary clinical diagnoses comprised eight hepatoblastoma (HB) and one hepatocellular neoplasm, not otherwise specified (HCN, NOS). Of the eight HB tumors, five were epithelial with variable fetal and embryonal components, two were mixed epithelial-mesenchymal, and one was epithelial-mesenchymal-teratoid HB. This information is summarized in Table 1. One patient (#7) underwent concurrent post-therapy resection and lung metastasectomy; both of which served as sources for two distinct PDX models (7.1 and 7.2, HB66, Table 2). Thus, overall, we generated ten PDX models representing nine patients.

Two out of nine patient samples (22.2%) showed ≥ 75% fetal component; however, the corresponding PDX models did not show any fetal differentiation. Similarly, four patient samples showed ≥ 50% embryonal component and only one of their PDX models showed proportionate or similar embryonal differentiation. Blastemal, mesenchymal and teratoid components were poorly represented in the patient samples and not seen in the PDX models. On the contrary, significant pleomorphic component, defined as > 50% of sampled tumor, was seen in three (33.3%) patients and overrepresented in PDX models (6 out of 10, 60%). Two models generated from the metastatic disease (PDX ID 7.2 and 9) resembled their corresponding patient tumor more closely with absent or minor pleomorphic component. Mitoses per 10 hpf ranged from 1 to 35 (mean 10.6) for patient samples and 5 to 70 (mean 26.6) for PDX models. Mitoses were always higher in the PDX models than the corresponding patient samples. Two patients (#2, 6) with a dominant fetal component ranging from 80 to 90% showed 1 to 7 mitoses per 10 hpf and their corresponding PDX models also showed generally low mitoses ranging from 6 to 28/10 hpf. Mean PDX mitoses of fetal dominant tumors was almost half (17/ 10 hpf) compared to embryonal dominant tumors (29.3/10 hpf), suggesting that even though definitive histologic fetal differentiation was not seen in many of these PDX models, the overall proliferative rate was still lower in the PDX models derived from fetal dominant tumors. (Fig. 2, Table 2).

Three of 10 PDXs (#2, 4, 5) were selected for immunophenotypic analyses, including three consecutive generations of each, making a total of 9 PDX models studied with a variety of immunohistochemical markers. (Figs. 3–5) Immunohistochemical markers such as Glypican-3 (GPC-3), Beta-catenin, AFP, Arginase, EPCAM, CK7, CK19, p53, glutamine synthetase (GS), Hepar, and Sox9 were chosen based on prior studies showing reactivity of hepatocellular tumors to these markers as described in the discussion. Significant concordance in the form of all 3 generations of PDX showing a score of + /- 1 of the corresponding patient sample; was seen for CK7, CK19, Ki-67 and p53 in all 3 patient-PDX model pairs. (Fig. 3) It was seen for Beta-catenin and Sox9 in 2 models, and for AFP, Arginase, GPC-3, and EPCAM in one model each. (Figs. 4 and 5) GS and Hepar did not show significant concordance in any model. Moderate concordance as defined by 2 of 3 generations with a score of + /- 1 of the corresponding patient sample; was seen for GPC-3 in 1 model and for GS in 2 models, while Hepar was the least concordant of all antibodies tested. (Table 3).

4. Discussion

HB is the most common malignant hepatocellular tumor in children, with some studies showing the highest percent increase in annual incidence over the past decade [14]. Currently, cisplatin and doxorubicin-based chemotherapy regimens are the primary treatment of choice. The lack of pre-clinical models has hindered the development of more effective and less toxic treatment strategies for patients with tumor recurrence and therapy resistance. PDXs are attempting to bridge this gap. Nicolle et al. established 24 PDX models from 20 HB, 1 HCC, 1 transitional cell tumor, and 2 malignant rhabdoid tumors by injecting fresh patient tumor cells into the interscapular brown fat of athymic nude mice in 2016 [15]. This was followed by the first demonstration of direct intrahepatic implantation of patient HB tumor tissue in immunodeficient mice (NSG and FRG) by Bissig-Choisat et al. in the same year [16]. This model recapitulated the histologic, genetic, and biological characteristics of the primary tumors, including metastatic behavior. Whitlock et al. have documented a detailed review of the developments in animal modeling of pediatric liver tumors [17]. Our study investigates comparative histologic and immunophenotypic characteristics of patients and corresponding murine PDX models generated by direct intrahepatic implantation of fresh tumors such as HB and HCN, NOS to shed light on how well these models represent the clinical patient samples.

HBs (including HCN, NOS) are embryonal tumors with well-recognized intra-tumor heterogeneity. Histologic differentiation includes fetal, embryonal, small cell undifferentiated, mesenchymal,

Table 1
Demographic and clinical details of the patients enrolled in this study.

Pt	Age (years)	Gender	Pre-surgical chemotherapy	Nature of specimen	Patient histologic diagnosis	AFP at sampling (ng/uL)
1	2	M	Yes	Explanted liver	Epithelial HB	21,800
2	1.3	M	No	Partial liver resection	Mixed epithelial, mesenchymal HB	> 207,200
3	4.36	M	Yes	Relapse in the allograft liver, needle biopsy	Epithelial HB	162
4	3.7	M	Yes	Partial liver resection	Mixed epithelial, mesenchymal, teratoid HB	157,000
5	4.3	M	No	Needle biopsy	Epithelial HB	785
6	1.3	M	No	Needle biopsy	Epithelial HB	439
7	3.4	M	Yes	Partial liver resection and Lung met resection	Mixed epithelial, mesenchymal, teratoid HB	37,300
8	7	M	Yes	Partial liver resection	HCN, NOS	> 207,200
9	5	F	Yes	Lung met resection	Epithelial HB	601

HCN, NOS-Hepatocellular neoplasm, not otherwise specified

Table 2
Comparative histology of the patient and PDX samples.

Patient/PDX							
PDX ID	Fetal	Embryonal	Blastema	Pleomorphic	Mesenchymal	Teratoid	Mitoses per 10 hpf
1-HB17	0/0	70/1	0/0	30/99	0/0	0/0	3/55
2-HB27	80/0	5/1	0/0	0/99	15/0	0/0	1/6
3-HB39	0/0	0/10	0/0	100/90	0/0	0/0	8/11
4-HB44	1/0	9/0	0/0	70/100	10/0	10/0	10/17
5-HB47	5/0	85/0	0/0	10/100	0/0	0/0	3/7
6-HB52	90/0	10/0	0/0	0/100	0/0	0/0	7/28
7.1-HB66 (primary)	10/90	60/9	10/0	0/1	10/0	10/0	2/7
7.2-HB66 (lung met)	10/10	60/0	10/0	0/0	10/90	10/0	2/5
8-HB106	5/0	5/90	0/0	90/10	0/0	0/0	35/40
9-HB113	1/0	99/80	0/0	0/20	0/0	0/0	27/70

Percentage of each component is indicated as patient/PDX - before and after the backslash, respectively.
*Two PDXs were generated from patient 7, one from the primary tumor and the second from the pulmonary metastatic lesion.

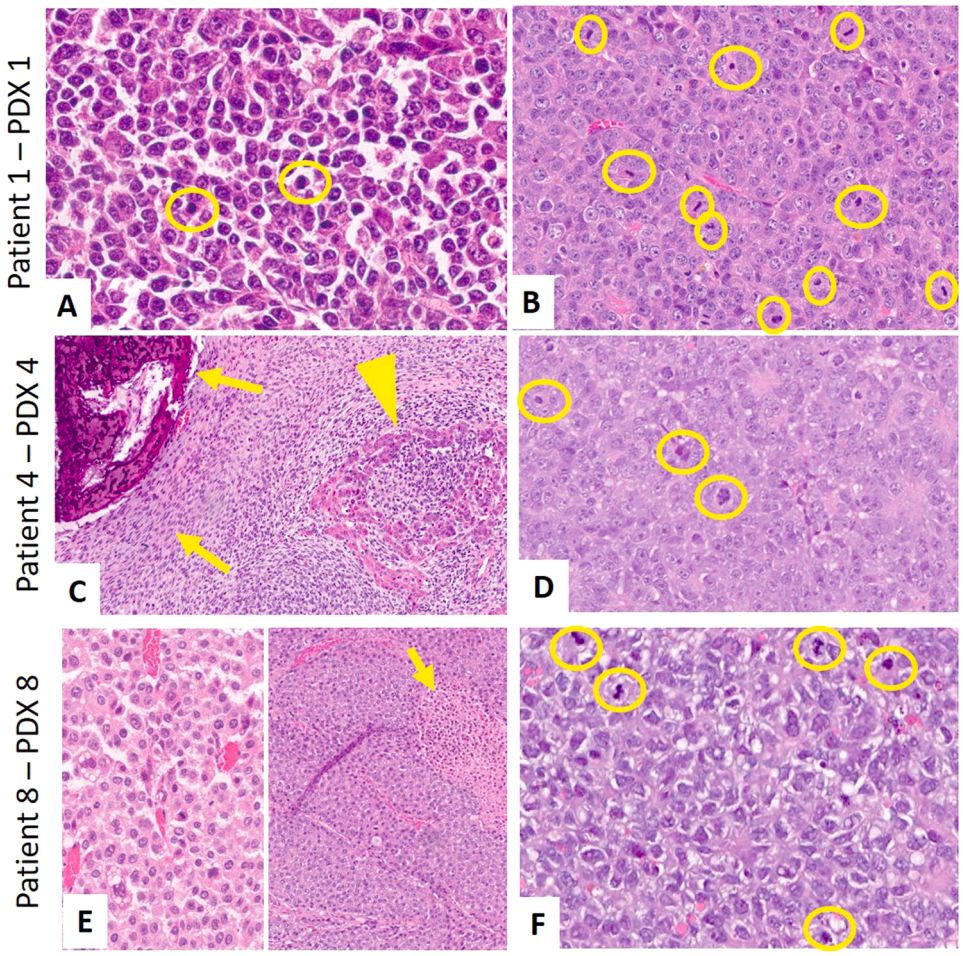

Fig. 2. Comparative histologic features of patient and PDX samples. A-B: Selected area from an embryonal component of patient 1 HB shows two mitotic figures (yellow circles). In a comparable area, the corresponding PDX sample showed 10 mitotic figures. C-D: Mixed epithelial-mesenchymal HB from patient 4 also led to a PDX with predominance of less differentiated or high grade component. Yellow arrows show mesenchymal component in the form of spindle cells and osteoid matrix. Yellow triangle shows fetal histology. E: Patient 8 with HCN, NOS shows a low grade fetal component on the left and a high grade macro trabecular HCC-like component on the right with a yellow arrow showing comedo necrosis. F: Corresponding PDX model shows a high grade, solid tumor with frequent mitoses in the PDX model. *All images H&E stained, panels C and E – 100x magnification, others 400x magnification.*

teratoid, and less often pleomorphic components. An ideal PDX model should be comparable to the patient sample in proportionate representation of each of these histologic components. However, that is not always true. Tissue used for PDX is harvested randomly from the patient tumor sample with a goal to obtain viable tumor. Specific tumor differentiation (fetal vs. embryonal vs. any other) cannot be selected during tissue harvest. Hence specific components used for PDX generation are not known upfront, which can affect the final histologic composition of the PDX tumor. Previous studies have shown variable representations of both fetal and embryonal components in their PDX

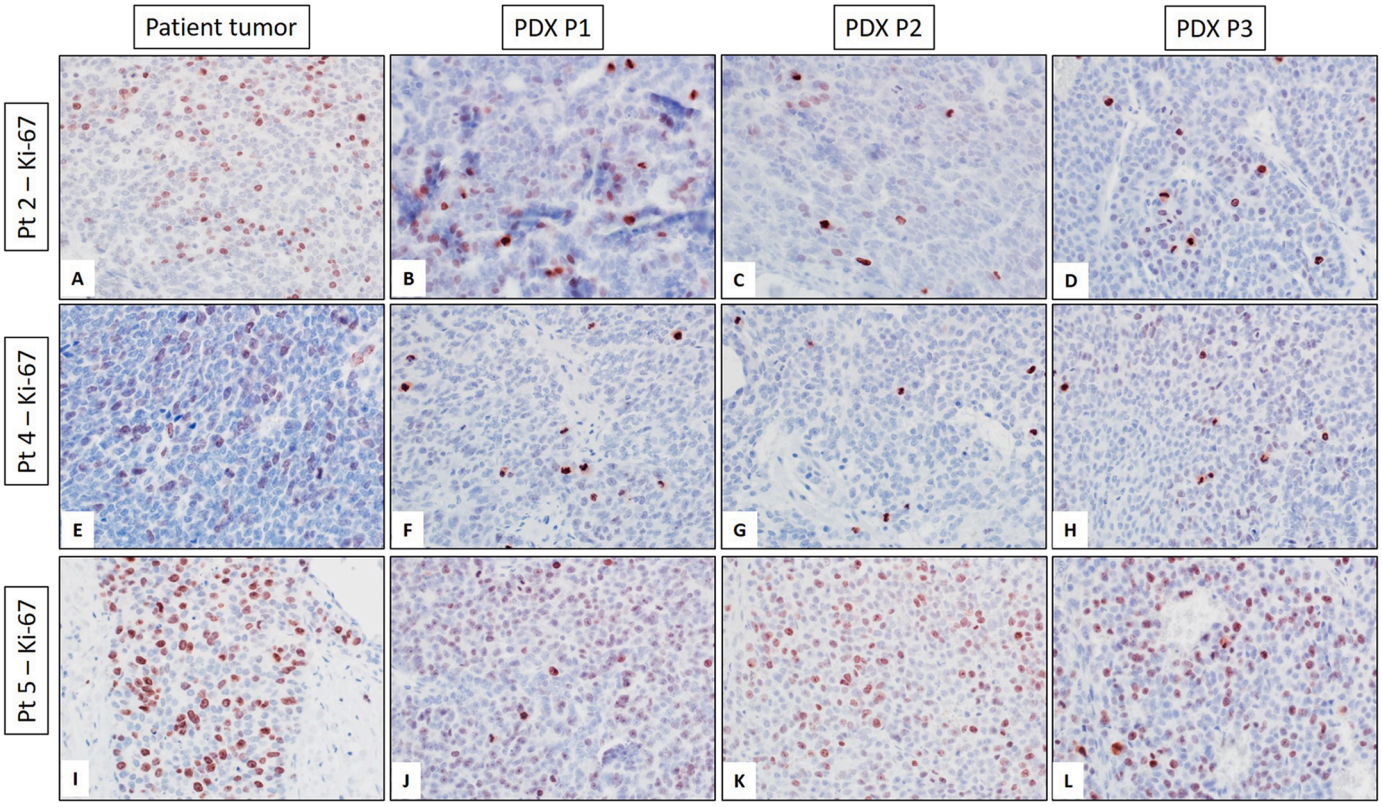

Fig. 3. Consistency of Ki-67 proliferation index between patient and corresponding PDX samples. Top and middle rows show samples from patients 2 and 5, respectively, where Ki-67 proliferation index was scored as 2 (1–25% cells positive) for both patient and 3 generations (P1, P2, P3) of PDX samples. Similarly, bottom row shows a sample from patient 6 where Ki-67 proliferation index was scored as 3 (25–75% cells positive) for both patient and 3 generations (P1, P2, P3) of PDX samples. *All images taken at 400x magnification.*

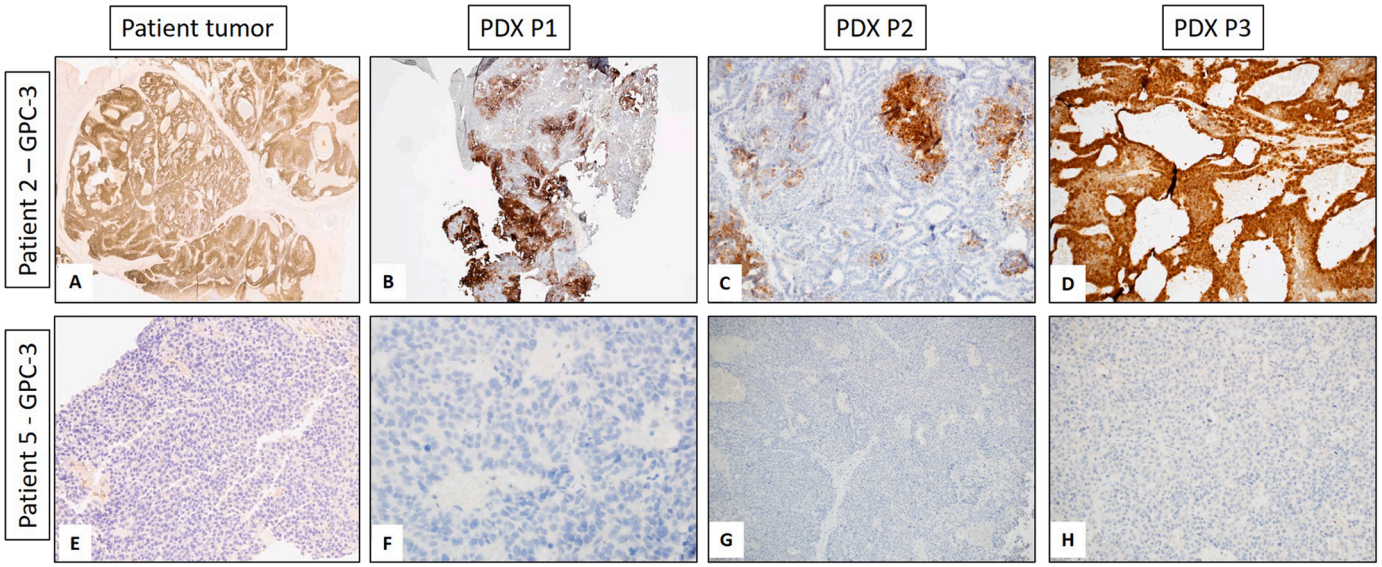

Fig. 4. GPC-3 expression in the PDX models. Top row shows PDX samples from a patient who had high GPC-3 expression (score 4), whereas bottom row shows PDX samples from patient 5 whose tumor was negative for GPC-3 (score 0). There was moderate concordance for patient 2 and high concordance for patient 5 for GPC-3 expression between the clinical sample and three generations of PDX samples. There was no apparent correlation between histology and GPC-3 expression. *All images except panel B taken at 40x magnification. Panel B taken at 20x magnification.*

models [16,17]. Fidelity of cancer cells in PDX models is an area of research with several studies on a variety of liver and non-liver tumor types showing aggressive phenotypes in PDX models compared to their corresponding patient samples [18]. Studies have also shown increasing aggressiveness of PDX models with serial generations [19–21]. These findings are not consistent with one study of 11 PDX models showing retained histopathologic, transcriptomic, and genomic characteristics of the original HCC biopsies over 6 generations [22]. Our PDXs showed an

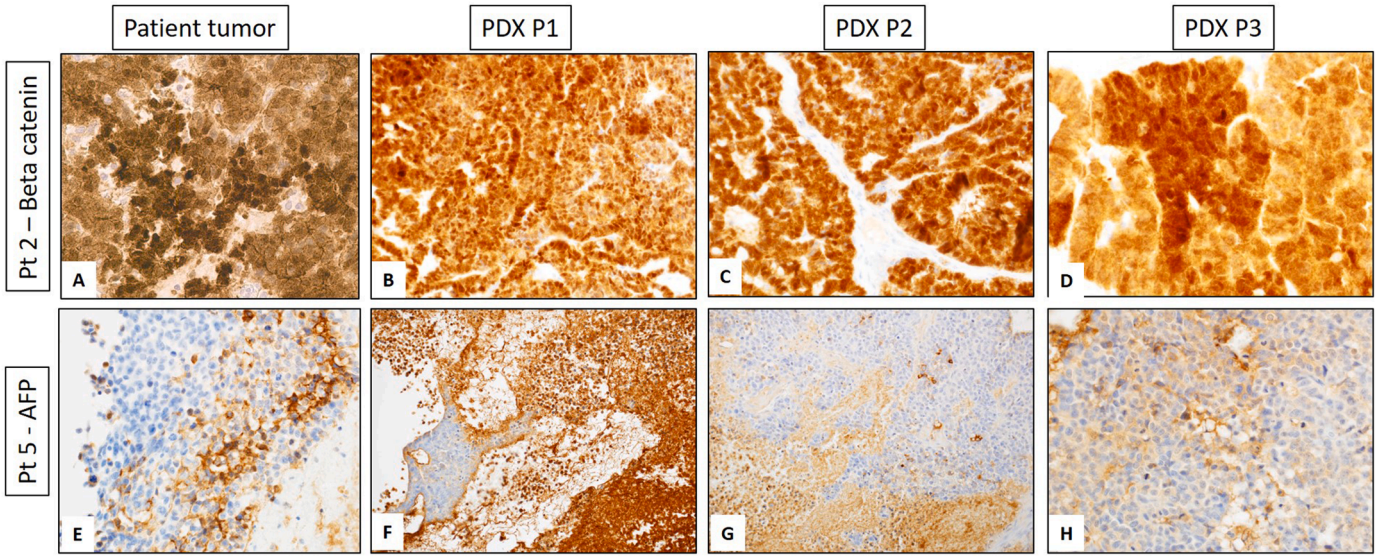

Fig. 5. Beta-catenin and AFP expression in tumor cells. Top row shows patient and 3 generations (P1 to P3) of corresponding PDX samples stained with immunohistochemical stain for Beta-catenin with consistently high nuclear and cytoplasmic expression among all samples. Bottom row shows patient and 3 generations (P1 to P3) of corresponding PDX samples stained with immunohistochemical stain for AFP with mild variability in cytoplasmic expression. *All images except panel F taken at 200x magnification. Panel F taken at 40x magnification.*

Table 3
Comparative immunophenotypic study of the patient-PDX sample pairs.

	Patient > PDX P1/P2/P3											
PDX ID	BCAT	GPC-3	AFP	GS	Arginase	CK7	CK19	Hepar	Sox9	Ki67	EPCAM	P53
2-HB27	4 > 4/4/4 **	4 > 3/2/4 *	4 > 2/2/2	2 > 2/1/0 *	2 > 0/2/3	0 > 0/0/0 **	0 > 0/0/0 **	4 > 1/0/2	1 > 4/4/3	2 > 2/2/2 **	0 > 0/2/2	0 > 1/1/1 **
4-HB44	1 > 4/3/4	1 > 4/4/4	1 > 3/1/3	0 > 2/3/1	0 > 2/2/2	0 > 0/0/0 **	0 > 0/0/0 **	0 > 2/3/3	2 > 3/2/3 **	2 > 2/2/2 **	0 > 2/1/1	0 > 1/1/1 **
5-HB47	4 > 4/4/4 **	0 > 0/0/0 **	2 > 3/1/2 **	0 > 1/0/2 *	2 > 2/1/1 **	1 > 0/0/0 **	0 > 0/0/0 **	2 > 3/1/0 *	4 > 4/4/3 **	3 > 3/3/3 **	0 > 1/1/1 **	0 > 1/1/1 **

AFP: Alpha feto protein; BCAT: Beta catenin; CK7: Cytokeratin 7; CK19: Cytokeratin 19; GPC-3: Glypican-3; GS: Glutamine synthetase
Immunohistochemistry score of the patient sample is followed by greater than sign (>) with subsequent 3 generations of PDXs separated by backslash (/).
* Indicates moderate concordance as defined by 2 of 3 generations with a score of + /- 1 of the corresponding patient sample
* *Indicates significant concordance as defined by all 3 generations of PDX showing a score of + /- 1 of the corresponding patient sample

over-representation of the higher grade tumor component as depicted by significant cytologic atypia and increased mitoses, resembling the pleomorphic component of HCN, NOS, or a poorly differentiated HCC. The average mitoses for patient samples was 9.7/10 hpf, compared to 22.3/10 hpf for PDXs. Ki-67 scores were comparable between patient and PDX samples, making them appropriate tools for testing of aggressive and therapy-resistant cases. Ki-67 scores did not show an increasing gradient over 3 generations of PDX models. This observation is overall consistent with the previous study of 24 PDXs generated from 20 patients by Nicolle et al. comprising of 20 HB, 1 HCN NOS, 1 HCC, and 2 malignant rhabdoid tumors. They also showed over-representation of the undifferentiated or pleomorphic component in the PDXs derived from primary tumors [15]. In their study, PDXs generated from intrahepatic recurrences or distant metastases resembled parental tumor histology more closely. Three of 10 PDxs in our study were generated from non-primary tumors (1 hepatic recurrence and 2 distant lung metastasis). Findings were slightly different in our series. Unlike Nicolle et al., our PDX model from the intrahepatic recurrence did show over-representation of the higher grade pleomorphic or undifferentiated component. However, similar to Nicolle et al., the 2 PDXs generated from the lung nodules (PDX 7.2 and 9) resembled metastatic tumor histology more closely and did not show significant pleomorphic component. In the intrahepatic model of Bissig-Choisat, both fetal and embryonal components were documented in the PDX model, along with one model showing focal mesenchymal differentiation in the form of osteoid-like material [16]. In comparison, only 2 out of our 10 PDXs showed a fetal component and only 1 showed definitive mesenchymal differentiation. A teratoid component was present in 2 patient tumors and absent in corresponding PDX models. One study had reported that HB tumors transplanted in the subcutaneous fat of athymic nude mice showed the transformation from pure epithelial to predominantly mesenchymal phenotype on serial passages [23]. We did not encounter a similar finding in our series.

Hepatoblastomas usually overexpress of Glypican-3 (GPC-3) detectable by microarray analysis [24] and corresponding strong and diffuse cytoplasmic reactivity by immunohistochemistry, along with negative staining in adjacent liver tissue [25]. GPC3 is an oncofetal protein anchored to the cell membrane normally expressed in the fetal liver but not in healthy adult livers [26]. Because of its overexpression, GPC3 has become a target molecule for many immunotherapy protocols [27]. Two out of 3 PDX models were concordant for GPC-3 expression in our study, making them eligible for immunotherapy related studies.

HBs are believed to be Wnt driven tumors with most common mutations in the *CTNNB1* gene that codes for the Beta-catenin protein manifesting as cytoplasmic and/or nuclear reactivity of Beta-catenin by immunohistochemistry. Two out of 3 PDX models showed significant concordance for Beta-catenin in our study. A third model from patient 4 showed a higher Beta-catenin expression score compared to the original

patient tumor. This patient sample was a mixed HB with epithelial, mesenchymal and teratoid components, with the later two being Beta-catenin weak or negative. In comparison, the PDX model was purely epithelial and mostly represented the pleomorphic component that was diffusely and strongly positive for Beta-catenin, leading to a higher score and an apparent discordance between the two.

Ki67 is an antigen encoding two protein isoforms that are present during all of the active cell cycle phases (G1, S, G2, and M) but absent in resting cells (G0). Coupled with its short half life of 1–1.5 hrs, this makes it a significant marker for cell proliferation and tumor aggressiveness [28]. Significant concordance of all 3 PDX models in our study is a promising finding suggesting that PDXs can accurately model proliferation rates of patient samples for specific studies of aggressive or high risk tumors.

Secreted AFP is a main serum protein during liver development [29] and, as serum AFP is often elevated in hepatoblastoma and hepatocellular carcinoma, its quantitation may be used for diagnosis, treatment monitoring, surveillance for disease recurrence, and prognostication [30]. Per CHIC (Children's Hepatic Tumors International Collaboration) risk stratification, AFP < 100 ng/ml at presentation is a high risk factor for HB [31]. In our clinical practice, it is not uncommon to encounter HB cases with markedly elevated serum AFP but weak or even negative staining in tumor cells. Only 1 out of 3 PDX models showed concordance for AFP expression by IHC, the rest being generally comparable. However, all 3 showed elevated human-AFP in the mice sera.

Other markers, such as GS, Arginase, CK7, CK19, Hepar, Sox9, EPCAM, and p53 have been uncommonly studied in HBs and have not shown consistent expression. Glutamine synthetase (GS) is a downstream target of the Wnt/beta-catenin pathway. Studies exploring the expression of glutamine synthetase in HB find that GS is expressed nearly universally across tumor cells of epithelial morphology but not in those of mesenchymal morphology [32,33]. Two of 3 PDX models showed moderate concordance for GS in our study and were the same as those with Beta-catenin concordance.

ARG1 staining has a high sensitivity (80–95%) and specificity (95–100%) for HCC, and it is also positive in HB, particularly in the fetal component [34]. Only 1 out of 3 PDX models showed concordance for arginase in our study.

CK7 is a membrane and cytoplasmic marker of biliary differentiation and its expression is typically negative in HB and HCC [35]. Only 1 of 3 patient samples showed weak expression of CK 7, and all PDXs were negative, suggesting that a cholangioblastic component is typically not present in the PDXs.

Cytokeratin-19 is often co-expressed with CK7. In a study involving HBs, CK19 staining was strong and diffuse in the embryonal components but weaker in the fetal [36]. It was uniformaly negative in all of our patient and PDX samples, again suggesting that our models did not show cholangioblastic differentiation.

Hepar is a monoclonal antibody that recognizes the mitochondrial antigen of hepatocytes and stains positively for both benign and malignant cells of hepatocytic origin. Its sensitivity and specificity for HCC is high [37,38]. Only 1 of 3 PDXs showed moderate concordance for Hepar. It was the least concordant antigen in our study.

Sox9 is involved in a number of important developmental and cancer pathways, including Wnt/Beta-catenin, Hedgehog, and Notch, and continues to be expressed in adult tissues, suggesting a role in cell maintenance and specification in adult life [39]. There is evidence to suggest that expression of Sox9 is a poor prognostic marker in HCC, [40] but it has not been studied in HB. Sox9 expression was variable in our study ranging from a score of 1 (fetal areas) to 4 (embryonal areas) in patient tumors. Two of 3 models showed significant concordance for Sox9.

EpCAM is a transmembrane glycoprotein known primarily for its role in mediating homotypic cell interactions in epithelial cells. In a study of 52 children with HB, it was shown to be stronger in embryonal areas, followed by crowded fetal and well-differentiated fetal [41]. EPCAM has been studied as a potential target for immunotherapy in HB [42]. EPCAM was negative in all 3 patient samples (including embryonal dominant) and showed low expression in PDX models with 1 model being significantly concordant.

The p53 tumor-suppressor protein, plays a crucial role in cancer prevention and both regulates and is regulated by pivotal cancer pathways such as Beta-catenin and Akt [43]. Staining patterns of strongly nuclear or totally absent p53 expression are associated with *TP53* mutations, which has been shown to be more common in poorly-differentiated HCC [44] and very rare in HB [45]. All 3 patient samples and PDX models showed a wild type pattern of p53 and were significantly concordant.

Most reported PDX models are derived from treated tumor samples during surgical resection. Resection samples are generally large and amenable to tissue harvesting for non-clinical purposes, such as PDX model development. Our series includes 3 out of 10 models (30%) generated from treatment naïve tumor tissue by harvesting a portion of tissue from diagnostic biopsies ($n = 2$) and resection ($n = 1$). This is typically only possible in centers with close collaboration between interventional radiology, surgery, pathology, and research laboratories. Tissue harvesting did not impede the ability to make a clinical diagnosis, or tissue archival for potential future studies.

5. Conclusion

This series details comparative histopathologic and immunophenotypic characteristics of patient tumors and corresponding intrahepatic PDX models of malignant pediatric hepatocellular tumors, including some derived from therapy naïve samples. Overall, PDX models appear to over-represent the higher-grade components of the original tumors and show significant concordance for proliferation rates, measured by Ki-67, making them appropriate tools to investigate new therapies for aggressive and therapy resistant cases. PDX models generated from therapy naïve tumor tissue offer unique opportunities to develop and test newer primary treatment regimens.

CRediT authorship contribution statement

Espinoza Andres: Data curation, Methodology, Validation, Writing – review & editing. **Patel Kalyani:** Conceptualization, Data curation, Formal analysis, Methodology, Supervision, Writing – original draft, Writing – review & editing. **Woodfield Sarah:** Data curation, Formal analysis, Investigation, Methodology, Supervision, Writing – review & editing. **Vasudevan Sanjeev:** Funding acquisition, Supervision, Writing – review & editing. **Lopez-Terrada Dolores:** Formal analysis, Funding acquisition, Investigation, Supervision, Writing – review & editing. **Sarabia Stephen:** Formal analysis, Investigation, Methodology, Validation, Writing – review & editing. **Major Angela:** Methodology, Project administration, Validation. **Patel Roma:** Methodology, Supervision, Validation. **Urbicain Martin:** Data curation, Methodology, Project administration, Software, Visualization, Writing – original draft, Writing – review & editing.

Declaration of Competing Interest

There is no conflict of interest.

Acknowledgment

This project was supported by the funding from the CPRIT Core Facility Support Award (CPRIT-RP180674).

Financial disclosure statement

There are no financial or other conflicts of interest for all the authors listed above, that could inappropriately influence (bias) their work for

this manuscript.

References

[1] J.A. Kahla, et al., Incidence and 5-year survival of children and adolescents with hepatoblastoma in the United States, Pedia Blood Cancer 69 (10) (2022) e29763.
[2] P. Sumazin, et al., Hepatoblastomas with carcinoma features represent a biological spectrum of aggressive neoplasms in children and young adults, J. Hepatol. 77 (4) (2022) 1026–1037.
[3] V. Ellerkamp, et al., Successful establishment of an orthotopic hepatoblastoma in vivo model in NOD/LtSz-scid IL2Rgammanull mice, PLoS One 6 (8) (2011) e23419.
[4] J. Zsiros, et al., Successful treatment of childhood high-risk hepatoblastoma with dose-intensive multiagent chemotherapy and surgery: final results of the SIOPEL-3HR study, J. Clin. Oncol. 28 (15) (2010) 2584–2590.
[5] P. Sivaprakasam, et al., Survival and long-term outcomes in children with hepatoblastoma treated with continuous infusion of cisplatin and doxorubicin, J. Pedia Hematol. Oncol. 33 (6) (2011) e226–e230.
[6] K. Watanabe, Current chemotherapeutic approaches for hepatoblastoma, Int J. Clin. Oncol. 18 (6) (2013) 955–961.
[7] J. Zsiros, et al., Dose-dense cisplatin-based chemotherapy and surgery for children with high-risk hepatoblastoma (SIOPEL-4): a prospective, single-arm, feasibility study, Lancet Oncol. 14 (9) (2013) 834–842.
[8] Y. Hata, et al., Establishment of an experimental model of human hepatoblastoma, Cancer 50 (1) (1982) 97–101.
[9] J.M. Schnater, et al., Subcutaneous and intrahepatic growth of human hepatoblastoma in immunodeficient mice, J. Hepatol. 45 (3) (2006) 377–386.
[10] L.C. Ong, et al., Effective inhibition of xenografts of hepatocellular carcinoma (HepG2) by rapamycin and bevacizumab in an intrahepatic model, Mol. Imaging Biol. 11 (5) (2009) 334–342.
[11] S.E. Woodfield, et al., A novel cell line based orthotopic xenograft mouse model that recapitulates human hepatoblastoma, Sci. Rep. 7 (1) (2017) 17751.
[12] P. Hingorani, et al., Trastuzumab deruxtecan, antibody-drug conjugate targeting HER2, is effective in pediatric malignancies: a report by the pediatric preclinical testing consortium, Mol. Cancer Ther. 21 (8) (2022) 1318–1325.
[13] M.E. Marques Da Costa, et al., A biobank of pediatric patient-derived-xenograft models in cancer precision medicine trial MAPPYACTS for relapsed and refractory tumors, Commun. Biol. 6 (1) (2023) 949.
[14] A.K. Hubbard, et al., Trends in international incidence of pediatric cancers in children under 5 years of age: 1988-2012, JNCI Cancer Spectr. 3 (1) (2019) pkz007.
[15] D. Nicolle, et al., Patient-derived mouse xenografts from pediatric liver cancer predict tumor recurrence and advise clinical management, Hepatology 64 (4) (2016) 1121–1135.
[16] B. Bissig-Choisat, et al., Novel patient-derived xenograft and cell line models for therapeutic testing of pediatric liver cancer, J. Hepatol. 65 (2) (2016) 325–333.
[17] R.S. Whitlock, et al., Animal modeling of pediatric liver cancer, Cancers 12 (2) (2020).
[18] J. Shi, et al., The fidelity of cancer cells in PDX models: characteristics, mechanism and clinical significance, Int J. Cancer 146 (8) (2020) 2078–2088.
[19] C.S. Wegner, et al., Increasing aggressiveness of patient-derived xenograft models of cervix carcinoma during serial transplantation, Oncotarget 9 (30) (2018) 21036–21051.
[20] A.T. Pearson, et al., Patient-derived xenograft (PDX) tumors increase growth rate with time, Oncotarget 7 (7) (2016) 7993–8005.
[21] M.A. Gomez-Munoz, et al., Analysis of serial neuroblastoma PDX passages in mice allows the identification of new mediators of neuroblastoma aggressiveness, Int J. Mol. Sci. 24 (2) (2023).
[22] T. Blumer, et al., Hepatocellular carcinoma xenografts established from needle biopsies preserve the characteristics of the originating tumors, Hepatol. Commun. 3 (7) (2019) 971–986.
[23] C. Desdouets, et al., Proliferation and differentiation of a human hepatoblastoma transplanted in the Nude mouse, J. Hepatol. 23 (5) (1995) 569–577.
[24] J.H. Luo, et al., Transcriptomic and genomic analysis of human hepatocellular carcinomas and hepatoblastomas, Hepatology 44 (4) (2006) 1012–1024.
[25] D.L. Zynger, et al., Expression of glypican 3 in hepatoblastoma: an immunohistochemical study of 65 cases, Hum. Pathol. 39 (2) (2008) 224–230.
[26] F. Zhou, et al., Glypican-3: a promising biomarker for hepatocellular carcinoma diagnosis and treatment, Med Res. Rev. 38 (2) (2018) 741–767.
[27] T. Nishida, H. Kataoka, Glypican 3-targeted therapy in hepatocellular carcinoma, Cancers 11 (9) (2019).
[28] L.T. Li, et al., Ki67 is a promising molecular target in the diagnosis of cancer (review), Mol. Med. Rep. 11 (3) (2015) 1566–1572.
[29] V.N. Evdokimova, L.H. Butterfield, Alpha-fetoprotein and other tumour-associated antigens for immunotherapy of hepatocellular cancer, Expert Opin. Biol. Ther. 8 (3) (2008) 325–336.
[30] M.J. Murray, J.C. Nicholson, alpha-Fetoprotein, Arch. Dis. Child Educ. Pract. Ed. 96 (4) (2011) 141–147.
[31] R.L. Meyers, et al., Risk-stratified staging in paediatric hepatoblastoma: a unified analysis from the Children's Hepatic tumors International Collaboration, Lancet Oncol. 18 (1) (2017) 122–131.
[32] W.J. Huang, J.H. Tsai, Y.M. Jeng, Complementary roles of beta-catenin and glutamine synthetase immunostaining in diagnosis of chemotherapy-treated and untreated hepatoblastoma, J. Formos. Med. Assoc. 116 (7) (2017) 549–553.
[33] A. Schmidt, et al., Differential expression of glutamine synthetase and cytochrome P450 isoforms in human hepatoblastoma, Toxicology 281 (1-3) (2011) 7–14.
[34] Z.E. Chen, F. Lin, Application of immunohistochemistry in gastrointestinal and liver neoplasms: new markers and evolving practice, Arch. Pathol. Lab Med. 139 (1) (2015) 14–23.
[35] D. Dum, et al., Cytokeratin 7 and cytokeratin 20 expression in cancer: a tissue microarray study on 15,424 cancers, Exp. Mol. Pathol. 126 (2022) 104762.
[36] M.M. Cajaiba, et al., Hepatoblastomas and liver development: a study of cytokeratin immunoexpression in twenty-nine hepatoblastomas, Pedia Dev. Pathol. 9 (3) (2006) 196–202.
[37] M.S. Shiran, et al., The utility of hepatocyte paraffin 1 antibody in the immunohistological distinction of hepatocellular carcinoma from cholangiocarcinoma and metastatic carcinoma, Malays. J. Pathol. 28 (2) (2006) 87–92.
[38] Y. Takahashi, et al., Application of immunohistochemistry in the pathological diagnosis of liver tumors, Int J. Mol. Sci. 22 (11) (2021).
[39] A. Jo, et al., The versatile functions of Sox9 in development, stem cells, and human diseases, Genes Dis. 1 (2) (2014) 149–161.
[40] X. Guo, et al., Expression features of SOX9 associate with tumor progression and poor prognosis of hepatocellular carcinoma, Diagn. Pathol. 7 (2012) 44.
[41] O. Lopez-Nunez, S. Ranganathan, Immunohistochemical expression analysis of EpCAM in hepatoblastomas, Appl. Immunohistochem. Mol. Morphol. 28 (9) (2020) 711–718.
[42] S. Armeanu-Ebinger, et al., Targeting EpCAM (CD326) for immunotherapy in hepatoblastoma, Oncoimmunology 2 (1) (2013) e22620.
[43] M. Oren, Decision making by p53: life, death and cancer, Cell Death Differ. 10 (4) (2003) 431–442.
[44] T. Oda, et al., p53 gene mutation spectrum in hepatocellular carcinoma, Cancer Res. 52 (22) (1992) 6358–6364.
[45] T.C. Chen, L.L. Hsieh, T.T. Kuo, Absence of p53 gene mutation and infrequent overexpression of p53 protein in hepatoblastoma, J. Pathol. 176 (3) (1995) 243–247.